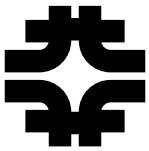

Fermi National Accelerator Laboratory

FERMILAB-Conf-95/147

Results on Fermilab Main Injector Dipole Measurements

B.C. Brown, R. Baiod, J. DiMarco, H.D. Glass, D.J. Harding, P.S. Martin,
S. Mishra, A. Mokhtarani, D.F. Orris, A. Russell, J.C. Tompkins and D.G.C. Walbridge

Fermi National Accelerator Laboratory
P.O. Box 500, Batavia, Illinois 60510

June 1995

Presented at the *Fourteenth International Conference on Magnet Technology*,
Tampere, Finland, June 11-16, 1995

Disclaimer

Results on Fermilab Main Injector Dipole Measurements

B.C. Brown, R. Baiod, J. DiMarco, H.D. Glass, D.J. Harding, P.S. Martin, S. Mishra,
A. Mokhtarani, D.F. Orris, A.D. Russell, J.C. Tompkins, and D.G.C. Walbridge
Fermi National Accelerator Laboratory, Batavia, Illinois, USA

Abstract—**Measurements of the productions run of Fermilab Main Injector Dipole magnets is underway. Redundant strength measurements provide a set of data which one can fit to mechanical and magnetic properties of the assembly. Plots of the field contribution from the steel supplement the usual plots of transfer function (B/I) *vs.* I in providing insight into the measured results.**

I. Introduction

By properly casting the fundamental equations which govern the strength of a multipole magnet, and using that to guide data presentation, one can achieve insight into magnet performance more reliably than by only comparing measured data to model calculations. We will emphasize presentations which reveal the features which govern magnet strength.

Since the field in an electromagnet is produced by current and by magnetic materials, it is not surprising that different views of the data will be required to clearly reveal the different contributions. In particular, care must be taken to present the effect due to the magnetization of the materials since these are typically a small part of the total field in a well designed magnet.

II. Measurement Fundamentals

A. Steel Magnets with Air Gaps

We employ Ampere's Law to predict magnetic fields. We will apply it to a magnet with cross section as shown in Figure 1. If we separate the contribution of the gap from that of the steel,

$$\int_g \frac{\vec{B_g}}{\mu_0} \cdot d\vec{\ell} + \int_{\mathcal{L}} \vec{H} \cdot d\vec{\ell} \; = NI \tag{1}$$

where g represents the path in the air gap and $\mathcal{L}$ represents the path through the steel. For a dipole the integral across

Manuscript received June 12, 1995.
Work supported by the U.S. Department of Energy under contract No. DE-AC02-76CH03000.

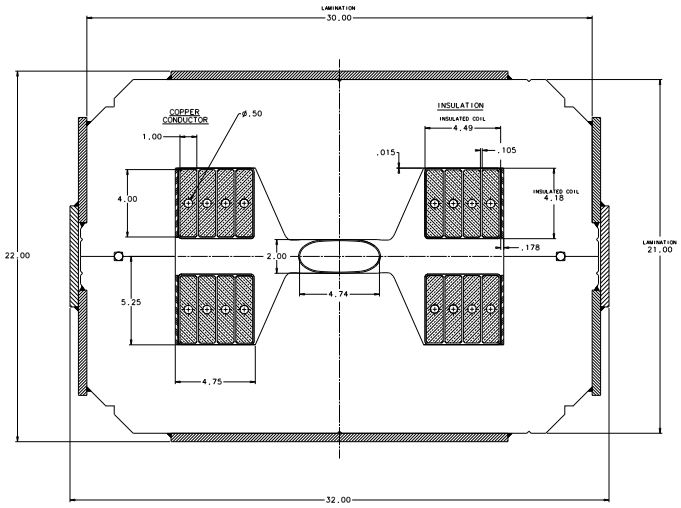

Fig. 1. Cross section of Main Injector Dipole with dimensions shown in inches. A flux line which begins near the center of the gap will have a length in the gap $g = 2$ inches (.0508 m) and a length in the iron $\mathcal{L} = 30$ inches (1.524 m)

the (uniform) field of the gap yields $B_1 g$.

$$\int_{\mathcal{L}} \vec{H} \cdot d\vec{\ell} \; = NI - \frac{B_1 g}{\mu_0}. \tag{2}$$

Evaluation and interpretation of the path integral is easiest when one follows a flux line thru the iron yoke. If we denote the path length thru the iron as $\mathcal{L}$ and the average of $\vec{H}$ as $< H >$ we find that the equation has now become

$$< H > \mathcal{L} = NI - \frac{B_1 g}{\mu_0}. \tag{3}$$

$$B_1 = \mu_0 \frac{NI}{g} - \mu_0 < H > \frac{\mathcal{L}}{g}. \tag{4}$$

We interpret Equation 4 via Figure 2. The iron magnetization curve is plotted as B *vs.* $\mu_0 H$. The linear relation of Equation 4 provides a "load line" on this plot with the operating point given by the intersection of the "load line" with the appropriate leg (increasing or decreasing H) of the hysteresis curve. The intercept at $< H >= 0$ is set by the current and geometry. The drop (or increase) in B in following the load line to its intersection with the steel property curves is interpreted as field due to the iron.

For the purposes of relating to measurement data with full length coils, let us integrate Equation 4 along the

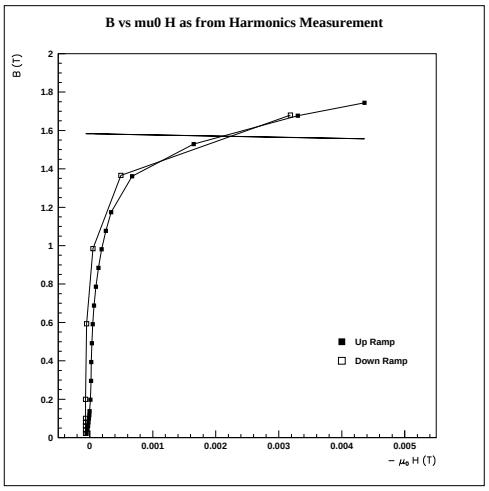

Fig. 2. B *vs.* $\mu_0 H$ for increasing and decreasing excitation. These loops are asymmetric in H, extending from $H = 0$ to $H = H_{max}$. Also shown is a Load Line for a Main Injector Dipole at an intermediate current. (see text).

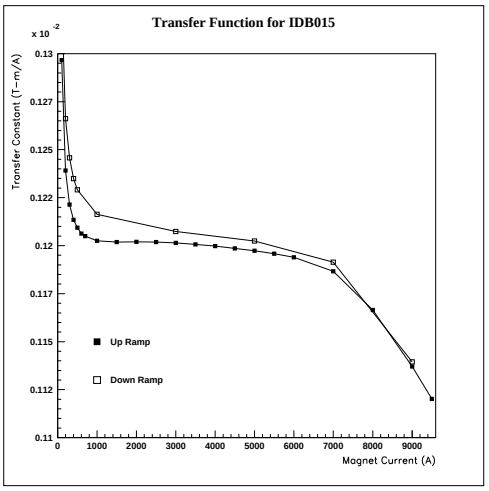

Fig. 3. Transfer Function $(\int B_1\, dl/I)$ *vs.* current for a 6-m Main Injector Dipole. Transfer Function is defined as the ratio of the integrated dipole field to the measured current.

length of a dipole.

$$\int_{-\infty}^{\infty} B_1(z)\, dz \; = B_1 L_{eff} = \mu_0 \frac{NI}{g} L_{eff} - \mu_0 < H > \frac{\mathcal{L}}{g} L_{eff}. \tag{5}$$

We refer to the this integral as the integrated dipole strength and this is what the measurement system is designed to record.

B. Main Injector Dipole Measurement System

Measurements are underway to monitor the production of the dipoles[1][2] [3][4] for the Main Injector Project[5] at Fermilab. A rotating coil Harmonics system measures both field strength and field shape at selected currents by integrating the changes with angle of the flux generated in suitable coil combinations[4][6]. A Flatcoil[7] system measures the shape of the field by integrating flux changes while translating a coil transverse to the beam direction. It determines magnet field strength by integrating the flux changes during ramping[1]. For production measurements, both systems are implemented using coils which extend sufficiently beyond the magnet ends to measure the full integral for each magnet. The measurement system[8] records data in a database[9] for further analysis and presentation.

C. Data Presentation

Accelerators demand field strength uniformity of order 0.1% - 0.01% Thus, if one plots the measured field or field integral *vs.* current for an iron dominated magnet, the nearly linear dependence is demonstrated but the plot is not very useful for observing deviations from ideal behavior. A traditional data presentation is shown in Figure 3 where we present the results from the Harmonics measurement system as a transfer function. The value of the transfer function in the region where it is constant provides a measure of the geometry of the magnet. The transfer function drops in value at high field due to magnet saturation and this is easily observed in this plot.

[1] This does not directly monitor the remanent field, of course.

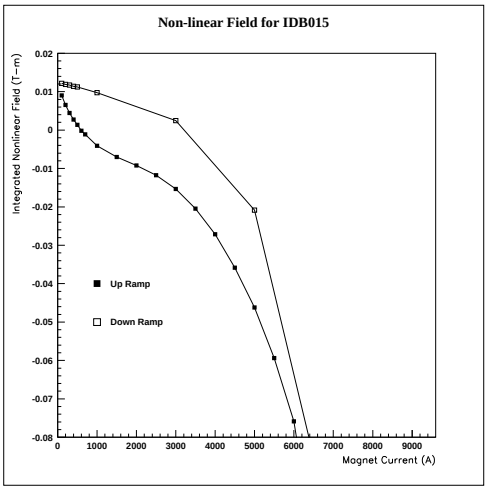

Fig. 4. Non-linear Integrated Field is the measured field minus that which would be produced with the same geometry and ideal $(\mu = \infty)$ iron. For this plot the effective length is taken as 6.10305 m from the the average determined from a selection of dipoles. The gap is assumed to be .0508508 m (2.002 inches) for this illustration. The design gap is 2.000 inches. The observed laminations provide nearly this value based on their largest extent, however, some additional material will be missing due to tearing rather than shearing in the die stamping process.

A plot which provides more information on the fields produced by the iron, especially at low excitation, can be constructed based on rearranging the above equation for magnet strength.

$$B_1 L_{eff} - \mu_0 \frac{NI}{g} L_{eff} = -\mu_0 < H > \frac{\mathcal{L}}{g} L_{eff}. \tag{6}$$

A plot of the left hand side of this equation *vs.* measured current shows directly the field contribution of the iron. We show this in Figure 4. Note the this scale reveals most of the details of the field strength.

D. Fitting for Magnet Geometry

To compare measurements with realistic expectations for magnet performance with maximal sensitivity, it is desired to separate geometric effects from iron properties. It would be desirable to simultaneously fit the full data set but we settle for a simpler system which is more easily implemented. Measurements involving a region where the $B-H$ curve is linear, will show a completely linear magnet excitation curve. Such a region is the final portion of the down ramp of a typical excitation curve and corresponds to a portion of the $B-H$ curve which is in the second quadrant[2]. We express this assumption as

$$B = \mu_0 \mu_{dr}(H + H_c). \tag{7}$$

We apply this by explicitly assuming the the B in the iron is also the B_1 in the gap. Solving this equation for H and substituting into Equation 6 we solve again for $B_1 L_{eff}$.

$$B_1 L_{eff} = \mu_0 L_{eff} \frac{NI}{g(1+\frac{\mathcal{L}}{g\mu_{dr}})} - \mu_0 L_{eff} \frac{\mathcal{L}}{g(1+\frac{\mathcal{L}}{g\mu_{dr}})} H_c \tag{8}$$

A linear fit of $B_1 L_{eff}$ *vs.* I for a portion of the measured curve will provide information on the H_c and L_{eff}/g.

[2]This description applies to unipolar ramps such as are characteristic of accelerator operation. If reversible power supplies are available, the same linear portion may extend for some distance in the third quadrant of the B-H curve.

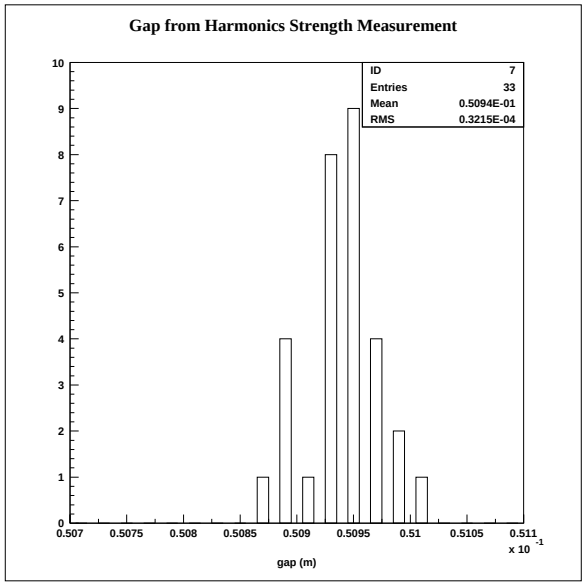

Fig. 5. Distribution of gaps for a selection of Main Injector Dipoles from a linear term in a fit of $B_1 L_{eff}$ *vs.* I. We use $L_{eff} = 6.103$ from an average based Hall/NMR Scans at 7000 A. No correction is applied for finite μ_{dr}.

However, the geometric term will have a small correction for the differential μ_{dr} of the steel. For the geometry of the Main Injector this correction is about 0.42% for a value $\mu_{dr} = 7000$. Having determined the critical geometric parameters and some of the magnetic parameters, one can proceed to a more elaborate fit. Instead, one may choose to simply examine the data based still on Equation 6.

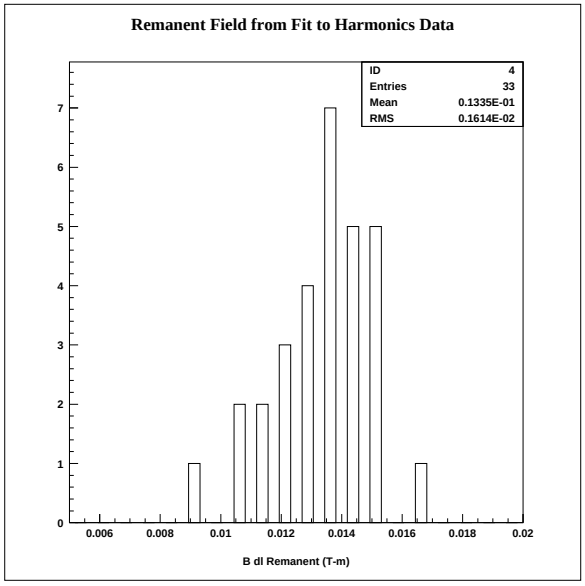

Fig. 6. Distribution of integrated field at 0 A current for a selection of Main Injector Dipoles as determined from the constant term in a quadratic fit of $B_1 L_{eff}$ *vs.* I.

III. Results for Main Injector Dipoles

We have applied the above analysis to a selection of the available data on Main Injector Dipoles. The portion of the down ramp which appears to be useable for the linear fit extends from above 2000 A (0.4 T) down to 0 A. Unfortunately, the most suitable data set is sparse in the region so we extend to fit the data point at 3000 A, including a quadratic term (which is observed to be small) to improve the quality of the fitting. We interpret the linear term without the correction for finite μ_{dr} as a gap as shown in Figure 5. We find a relative variance of the gap as determined in this way of 6.3×10^{-4}. We display the intercept from this fit as simply a field at 0 A excitation. This is shown in Figure 6.

Examining plots of the non-linear field provides insight into the properties of the steel in these dipole. In Figures 7 and 8 we display results from four sequential 6-m Main Injector dipoles. The Flatcoil measurement suppresses the remanent field. We see that in that case, the downramp strength measurements agree very precisely at low fields when the linear (geometric) term is subtracted, clearly confirming the hypothesis of the fit. More interesting is the agreement among measurements with the Har-

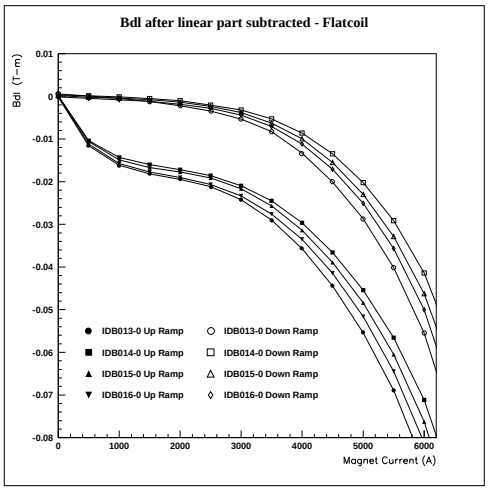

Fig. 7. Nonlinear portion of integrated dipole for four 6-m Main Injector dipoles as measured by the Flatcoil measuring system.

monics system at moderate fields on the upramp (near 1500 A). Here we see that the excitation has nearly cancelled the differences which are apparent at 0 A. This is a property of the underlying $B - H$ curves.

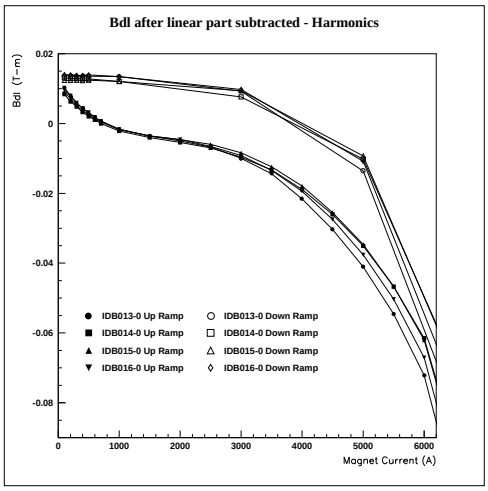

Fig. 8. Nonlinear portion of integrated dipole for four 6-m Main Injector dipoles as measured by the Harmonics measuring system.

These plots at intermediate fields are of special interest to the Main Injector as they demonstrate that the variations of the steel properties at intermediate excitation ($\mu_0 H \sim 0.002$ T) are significant. These magnets sample steel from a variety of processing runs and the resulting strength variations, while not serious, have focused attention on the uniformity of the steel processing. Presentation of measured data compared to average properties[4] is effective in discerning any troubling trends. These plots, however, permit one to clearly establish the significant differences as due to steel.

IV. Discussion and Suggestions for Further Work

By using the fundamental relations which govern the strength of magnets, analysis strategies have been developed which provide insight from measurement results. This work applies directly to strength measurements of quadrupole, sextapoles other magnet designs. The implicit assumption that B is constant along a flux line is a crude approximation, but that is not a limitation in using this to examine measurement data. Extending this work to explicitly consider laminations provides insight into the interaction of packing factor and and magnet saturation but that will have to remain for later consideration.

V. Acknowledgements

This work is based on discussions with Klaus Halbach which began at the US Particle Accelerator School in January 1993. We gratefully acknowledge the contributions of the MTF staff.

References

[1] D. J. Harding *et. al.* Design Considerations and Prototype Performance of the Fermilab Main Injector Dipole. In *Conference Record of the 1991 IEEE Particle Accelerator Conference, San Francisco, May 6-9, 1991*, page 2477. Institute of Electrical and Electronic Engineers, 1991.

[2] M. E. Bleadon *et. al.* The Fermilab Main Injector Dipole: Construction Techniques and Prototype Magnet Measurements. *IEEE Trans. on Mag.*, MAG-28:160, 1992. Proceeding of the 12th International Conference on Magnet Technology, Leningrad, USSR, 24-28 June 1991.

[3] B. C. Brown *et. al.* The Design and Manufacture of the Fermilab Main Injector Dipole Magnet. In P. Marin and P. Mandrillon, editors, *Proceedings of the Third European Particle Accelerator Conference*, volume 2, page 1376. Editions Frontieres, B.P. 33, 91192 Gif-sur Yvette Cedex, France, 1992. Technical University of Berlin, March 24-28, 1992.

[4] D.J. Harding *et. al.* Magnetic Field Measurements of the Initial Production Main Injector Dipoles. In *Conf. Record of 1995 IEEE Particle Accel. Conf.(to be published).*

[5] D. Bogert. The Fermilab Injector Complex. In *Conf. Record of 1995 IEEE Particle Accel. Conf.(to be published).*

[6] Bruce C. Brown. Fundamentals of Magnetic Measurements with Illustrations from Fermilab experience. In P. F. Dahl, editor, *Proceedings of the ICFA Workshop on Superconducting Magnets and Cryogenics*, page 297. Brookhaven National Lab, May 1986.

[7] H.D. Glass *et. al.* Flatcoil Systems for Measurements of Fermilab Magnets. In *Proceedings This Conf.*

[8] J.W. Sim et al. Software for a Database-Controlled Measurement System at the Fermilab Magnet Test Facility. In *Conf. Record of 1995 IEEE Particle Accel. Conf.(to be published).*

[9] J.W. Sim et al. A Relational Database for Magnets and Measurement Systems at the Fermilab Magnet Test Facility. In *Conf. Record of 1995 IEEE Particle Accel. Conf.(to be published).*